Journal of Power Sources 195 (2010) 3250–3255

Contents lists available at ScienceDirect

Journal of Power Sources

journal homepage: www.elsevier.com/locate/jpowsour

Two-phase flow measurement system for polymer electrolyte fuel cells

Amir M. Niroumand*, Mehrdad Saif

Engineering Science Department, Simon Fraser University, Burnaby, BC, Canada

ARTICLE INFO

Article history:
Received 14 October 2009
Received in revised form
24 November 2009
Accepted 25 November 2009
Available online 1 December 2009

Keywords:
Two-phase flow
Membrane conditioning
Fuel cell
Diagnostics
Oscillation

ABSTRACT

In this paper, a sensory system capable of measuring two-phase flow of water at the PEFC output is introduced. It works based on collecting and evaporating the liquid water that exits the PEFC in a vessel that is heated to a temperature above that of the fuel cell temperature. By measuring the vessel dew point temperature and flow rate, the mass of water in liquid and vapor phases are calculated. To demonstrate the capabilities of this measurement system, it is placed at the output of a PEFC cathode during membrane conditioning. The effect of two-phase flow on cell voltage reveals two distinct modes of liquid water transport in the PEFC cathode during membrane conditioning.

1. Introduction

Polymer electrolyte fuel cells (PEFCs) are electrochemical cells that combine hydrogen and oxygen and produce electricity, heat, and water. The management of water is one critical factor affecting the performance and durability of PEFCs. The proton conductivity of the Nafion® membrane depends on its hydration level, and improves with higher water contents [1,2]. In addition, the water produced at the cathode catalyst cites need to be removed, otherwise, it would block the catalyst sites, gas diffusion layer (GDL) pores, and/or flow field channel [1]. This blockage is known as flooding, and results in fluctuations in the cell voltage [3–5]. The balance between membrane humidification and removal of the excess water is critical for optimal operation of PEFCs.

The water produced at the cathode can evaporate into the cathode stream and leave the PEFC. The evaporative water transport mechanism depends primarily on the temperature, humidity, and cathode flow rate. However, in most commercial fuel stacks, in order to improve membrane humidification conditions, both the anode and cathode streams are humidified before entering the PEFC. This results in the evaporative water transport out of the cell to be less than the produced water; causing a residual amount of liquid water to accumulate in the cathode. This liquid water is transported out of the cell using convective forces as slug flow. Therefore, water exhibits a two-phase flow in the cathode of PEM fuel cells, i.e., in vapor and liquid phases. Understanding the dynamics of this two-phase flow allows optimizing the PEFC design, and has been the subject of many works in this field. Following is a summary of approaches reported in the literature to understand two-phase flow.

Many authors have used modeling to better understand the two-phase water transport in PEFCs [6–13]. These models need to be validated using experimental measurements. However, the many degrees of freedom and parameters used to capture the two-phase transport properties in PEFCs result in an ill-posed parameter fitting problem. Direct measurement of two-phase flow is essential for understanding its dynamics as well as model validation. As a result, many techniques have been developed for this purpose. Following is an analysis of the techniques reported in the literature for direct measurement of two-phase water transport in PEFCs.

Magnetic resonance imaging (MRI) is a technique used to study spatial water distribution in PEFCs [14–17]. In this method, an array of RF transmitters and receivers is used to provide slices of two and a half dimensional images from the volume of interest. The high spatial resolution of MRI makes it an excellent tool for studying water profiles in the fuel cell membrane. The main short fall of this technique when applied to PEFCs arises from the fact that the magnetic inductive properties of carbon limits acquiring useful data from GDL and flow fields, unless alternative materials are used. Also similar to neutron imaging, MRI requires expensive hardware and is challenging to calibrate in order to quantify the amount of water in the PEFC.

An alternative approach is to use a transparent cathode to observe the transport of liquid water in the GDL and flow fields [4,18–23]. The visualization technique provides insight into the

* Corresponding author. Tel.: +1 604 782 4407.
E-mail address: amniroum@sfu.ca (A.M. Niroumand).

0378-7753/$ – see front matter © 2009 Elsevier B.V. All rights reserved.
doi:10.1016/j.jpowsour.2009.11.108

Nomenclature

F	Faraday constant, 96,500 C mol^{-1}
I	fuel cell current, A
n	number of species, mol
$\dot{n}$	flow rate, mol^{-1}
P	pressure, Pa
R	gas constant, 8.31 kJ^{-1} mol^{-1}
T	temperature, K
V	volume, m^3
$\dot{V}$	volumetric flow rate, m^3 s^{-1}

Subscript

a	anode
air	air
c	cathode
cell	fuel cell
dp	dew point
gas	gas (without water vapor)
in	vessel input
liq	liquid water
out	vessel output
T	total
v	vessel
vap	water vapor

mechanical behavior of water transport in the cathode; however, they have limited capability in terms of quantifying the amount of liquid water in the fuel cell. In addition, building the transparent cathode requires use of special materials, which have different heat transfer and surface tension properties than the fuel cell flow field. This in turn results in distortion in the observed water transport behavior.

Another method used to visualize spatial water accumulation and distribution in PEFCs cells is neutron imaging [24–30]. In this method, a neutron source and detector is placed on both sides of a PEFC anode and cathode flow fields. The neutron intensity measured by the detector changes proportional to the amount of water present in the fuel cell, revealing the spatial accumulation and transport of water in the fuel cell. In addition, the measured data can be calibrated to quantify the total amount of water. However, one shortfall of this method is that it can only measure the total amount of water in the cathode and anode, rather than separate measurements for the two electrodes water contents. In addition, the measurement would represent the total amount of water in both vapor and liquid phases, not distinguishing between the two. Finally, neutron imaging requires expensive hardware and is challenging to calibrate for reliable data quantification.

MRI, transparent flow field, and neutron imaging techniques explained above are more useful for phenomenological study of water transport in PEFCs. Other methods have been developed to quantify the two-phase water transport phenomena. The underlying technique in these methods is to measure the water balance in the PEFC. In this technique, the anode and cathode are supplied with reactants at a known humidity levels, and the water content of the output stream is measured [31–40]. The difference between the input and output water contents is used to quantify water transport in PEFCs. Since the stream leaving the fuel cell consists of a two-phase flow, measuring the vapor and liquid water components is a major challenge with water balance. Following is a brief review of various techniques reported in the literature used to make such measurements, along with their advantage and shortfalls.

Laser absorption spectroscopy is one method used to measure the water vapor partial pressure in the fuel cells [31–33]. As the water vapor partial pressure changes, so does the absorption rate of laser passing through the stream. This property is used to quantify the partial pressure of water vapor, and results in fast and reliable readings. It can also be integrated into the fuel cell to obtain spatial distribution of water vapor pressure within the cell. However, the short come of this method is that it cannot measure the amount of liquid water in the stream.

Gas chromatography is an alternative technique that is used to measure the concentration of water vapor in PEFCs [34–36]. In this method, a relatively small sample of the gas is taken from the fuel cell, and directed to the chromatograph for species concentration measurement. This method can too be integrated into the fuel cell to obtain spatial measurement of species concentration in the fuel cell; however, its limit also resides in the fact that it can only handle gas phase species. Therefore, liquid water concentration cannot be measured using gas chromatography.

Another technique used to quantify the water content of the fuel cell output stream is to condense the liquid water and measure its weight or volume [37,38]. This method results in the total amount of water leaving the cell. Therefore, in combination with other techniques that measure the water vapor pressure, e.g., laser absorption spectroscopy, it is possible to quantify the amount of water leaving the fuel cell in vapor and liquid phases. However, the shortfall of this method is that the mass/volume of the condensed water is relatively small. Therefore, in order for the measurement to fall within resolution of the measurement devices, measurements are obtained over long periods of time. This limits the temporal resolution of the measured data and the results can only reveal average transport properties. However, intermittent water transport in PEFC electrodes, e.g., slug flow, cannot be accurately quantified using this technique [22].

Solid state humidity sensors are an alternative device used to measure the relative humidity of the PEFC anode and cathode output streams [39,40]. These sensors measure changes in a stream capacitor dielectric constant and temperature to quantify its relative humidity (RH). Similar to laser absorption chromatography and gas chromatography, RH sensors can only measure water in the gas phase. In fact, when used with a saturated stream, water condensation on these sensors is one source of unreliable reading.

Table 1 summarizes the advantage and short come of the water measurement methods reported in the literature. It can be seen that none of these methods can quantify two-phase flow in PEFCs with high mass and temporal resolution. In the following section, a solid state humidity sensor based measurement system is

Table 1
Water measurement techniques used for PEM fuel cells.

Method	Ref.	Strength	Weakness
MRI	[14–17]	Membrane water distribution	Not compatible with carbon, expensive
Transparent cathode	[4,18–23]	Phenomenological study	Limited quantification
Neutron imaging	[24–30]	Non-intrusive, spatial water distribution	Measures anode + cathode, limited accuracy, expensive
Laser spectroscopy	[31–33]	Measure spatial distribution	Cannot measure liquid water
Gas chromatography	[34–36]	Spatial species distribution	Works only for gasses
Condensation	[37,38]	Total water balance	Small temporal resolution
Humidity sensor	[39,40]	Accurate, cheap	Measures only water vapor

introduced that has such capability. Next, the fuel cell hardware used to demonstrate the capabilities of the system is introduced. Finally, experimental results for two-phase flow measurement during membrane humidification are presented, followed by a discussion of the results.

2. Experimental setup

2.1. Two-phase flow measurement system

Liquid water can leave the fuel cell with a continuous flow or as intermittent bursts, e.g., slug flow [18]. Continuous liquid flow can be measured using various types of flow meters; however, it is more difficult to measure slug flow. The measurement system reported below is developed to specifically measure such flow dynamics.

In order to measure the amount of liquid water exiting the fuel cell, a Sensirion SHT75 solid state humidity sensor, with an RH accuracy of ±2% and temperature accuracy of ±1.5% over the range, was used in a heated stainless steel vessel, as shown schematically in Fig. 1. An Omega FGR-60 250W rope heater was used with an on-off controller to control the vessel heat with a full-scale accuracy of ±1%. A 125 W Omega FGR-30 rope heater was also used with an on-off controller to heat the connecting tubing. A Measurement Specialties Inc. US 10000 pressure transducer, with 0–50 psi range and ±0.05% full-scale accuracy, was used to measure the vessel pressure.

The above vessel is placed at the output of a fuel cell to measure two-phase flow as it exits the PEFC. When the vessel is dry and there is no liquid water in the PEFC output stream, the humidity sensor measurement corresponds to the partial pressure of water vapor at the fuel cell output at steady state. When bursts of liquid water exit the fuel cell, they accumulate in the vessel. This is because the diameter of the vessel is larger than the fuel cell output tubing. Since the vessel is heated to a temperature above that of the fuel cell output stream, the liquid water that is collected in the vessel evaporates in the stream passing through the vessel. During this evaporation period, the humidity sensor measurement shows higher water partial pressure in the vessel. When all the liquid water in the vessel is evaporated and the vessel is dried, the humidity sensor measurement again measures the partial pressure of water vapor in the fuel cell output at steady state. The total amount of liquid water can then be calculated from the humidity sensor measurements between two dried vessel conditions. These stages are shown schematically in Fig. 2.

In Fig. 2, times t_1 and t_2 correspond to two fully dried vessel states, between which liquid water is expelled into and evaporated

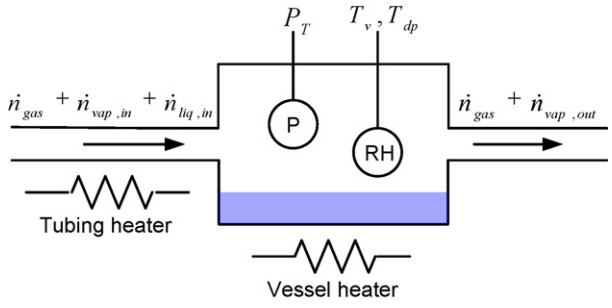

Fig. 1. Schematic of the sensory vessel for measurement of water content at the PEM fuel cell output. The pressure sensor, P, measures the total pressure in the vessel, P_T. The humidity sensor, RH, measures the temperature and dew point temperature inside the vessel, T_v and T_{dp}, respectively. The vessel input flow stream contains the gas(excluding water vapor), liquid water, and water vapor, $\dot{n}_{gas}$, $\dot{n}_{liq,in}$, and $\dot{n}_{vap,in}$, respectively. The vessel output stream contains gas and water vapor, $\dot{n}_{gas}$ and $\dot{n}_{liq,out}$, respectively. The tubing is heated to avoid condensation of water vapor. The vessel is heated to evaporate the liquid water.

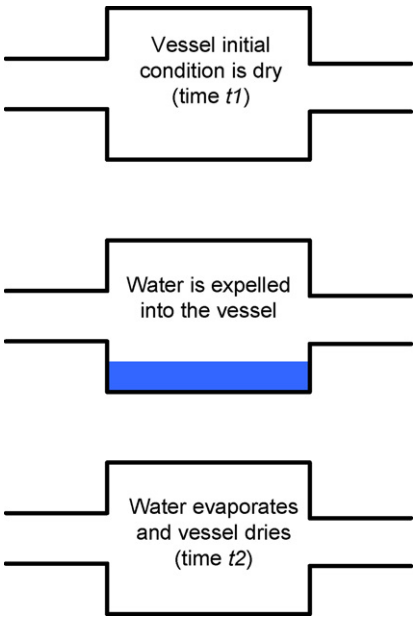

Fig. 2. Vessel dry initial and final conditions at times t_1 and t_2, required for measuring bursts of liquid water that occur between these times.

out of the vessel. If the vessel is taken as the control volume, the number of moles of liquid water expelled into the vessel, $n_{liq,in}$, between times t_1 and t_2 can be calculated using the following relationship:

$$n_{liq,in} = \int_{t_1}^{t_2} (\dot{n}_{vap,out} - \dot{n}_{vap,in})dt \ \text{(mol)} \quad (1)$$

with $\dot{n}_{vap,out}$ being the molar flow rate of total water vapor leaving the vessel, and $\dot{n}_{vap,in}$ the molar flow rate of water vapor entering the vessel.

In the above derivation, it is assumed that all the liquid water exits the vessel in vapor form, and not as liquid. However, if the total amount of water entering the vessel is larger than its storage capacity, the vessel would flood and the liquid water would directly exit the vessel without being evaporated. This volume for the vessel used in this experiment is 15 cm^3. In order to ensure that the vessel is not flooded, the humidity sensor is placed slightly below the vessel output opening, as seen schematically in Fig. 1. The humidity sensor is sensitive to liquid water, and would signal an error if in contact with liquid water. Therefore, if the vessel is flooded, liquid water will get in contact with the humidity sensor, which would result in an error signal. This way, it is possible to ensure that the vessel does not flood and therefore water does not leave the vessel in liquid form.

Assuming that water vapor and other gases obey the ideal gas law, the following relationships are true in the vessel at steady state conditions:

$$P_{vap}\dot{V}_{vap} = \dot{n}_{vap}RT_{vap} \quad (2)$$

$$P_{gas}\dot{V}_{gas} = \dot{n}_{gas}RT_{gas} \quad (3)$$

with P_{vap} and P_{gas} being the water vapor and gas partial pressures, $\dot{V}_{vap}$ and $\dot{V}_{gas}$ the water vapor and gas volumetric flow rates, $\dot{n}_{vap}$ and $\dot{n}_{gas}$ the molar flow rate of water vapor and reactant passing through the vessel, and T_{vap} and T_{gas} the water vapor and gas temperatures in the vessel, respectively. The volumetric flow rate and temperature of water vapor and gas in the vessel are equal, i.e., $\dot{V}_{vap} = \dot{V}_{gas}$ and $T_{vap} = T_{gas}$. Therefore, if Eqs. (2) and (3) are divided and rearranged, the following equation can be written for the molar flow rate of

water vapor passing through vessel:

$$\dot{n}_{vap} = \frac{\dot{n}_{gas} P_{vap}}{P_{gas}} \ (\text{mol}^{-1}) \quad (4)$$

In Eq. (4), the partial pressure of water in the vessel, P_{vap}, can be calculated from the humidity sensor dew point temperature reading, T_{dp}, using the following relationship [2]:

$$P_{vap} = 10^{-3.18+0.03T_{dp}-9.18\times10^{-5}T_{dp}^2+1.45\times10^{-7}T_{dp}^3} \ (\text{Pa}) \quad (5)$$

The partial pressure of gas in the vessel, P_{gas}, can be calculated as the difference between the partial pressure of water vapor and the vessel total pressure, P_T, measured by a pressure sensor in the vessel. When the vessel is placed at the output of a PEFC cathode, the molar flow rate of gas passing through the vessel, $\dot{n}_{gas}$, is equal to the molar flow rate of gas exiting the cathode. The molar flow rate of gas exiting the cathode can be calculated from the fuel cell input molar air flow rate, $\dot{n}_{air}$, and cell current, I, using the following relationship [1]:

$$\dot{n}_{gas} = \dot{n}_{air} - \frac{I}{4F} \ (\text{mol}^{-1}) \quad (6)$$

By substituting the values for the cathode output flow rate, partial pressure of water vapor and gas in Eq. (4), it is possible to calculate the molar flow rate of water vapor passing through the vessel, $\dot{n}_{vap}$. Assuming homogeneous saturation pressure in the vessel, $\dot{n}_{vap}$ is equal to the molar flow rate of water vapor exiting the vessel, $\dot{n}_{vap,out}$. When there is no liquid water in the vessel, and steady state conditions, $\dot{n}_{vap}$ is also equal to the molar flow rate of water vapor entering the vessel, $\dot{n}_{vap,in}$. By substituting these values for the molar flow rate of water vapor at the vessel input and output into Eq. (1), the number of moles of liquid water expelled into the vessel, $n_{liq,in}$, can be calculated.

In order to demonstrate the capabilities of the above measurement system, it was used at the output of a PEFC cathode during membrane humidification to measure the two-phase flow of water. The fuel cell system used for this purpose is explained next.

2.2. Fuel cell system

A single cell PEFC with an active area of 49 cm^2 and a commercially available 12 series ETek membrane electrode assemble (MEA) was used. The MEA consists of a Nafion 112 membrane and carbon supported platinum, with anode and cathode platinum loadings of 0.1 and 0.4 mg Pt cm^{-2}, respectively. A 200 μm Toray carbon paper was used for both anode and cathode GDLs. Cross-flow fields were used with 36 passes on the anode and 38 passes on the cathode side; with cross-section of 1 mm × 1 mm.

The cell temperature was controlled by circulating water into a separate pair of flow fields sandwiching the fuel cell. Anode and cathode input flow rates were controlled using mass flow controllers and the output pressures were controlled using back pressure control valves. Boiling humidifiers were used to humidify hydrogen and air entering the fuel cell. Hydrogen and air temperatures between the humidifier and the fuel cell were controlled using heating elements to avoid water condensation in the tubing. The anode and cathode input and output temperatures were also measured using K-type thermocouple with an accuracy of ±1.1 °C, placed in the input and output manifolds.

The fuel cell operating temperature was set at 80 °C to which results in optimal kinetics for the membrane used. Anode and cathode pressures were set at 20 psi, dew point temperatures of 40 °C, and input temperatures of 50 °C. These operating conditions are summarized in Table 2.

Table 2
Fuel cell operating values.

Parameter	Value
T_{cell} (°C)	80
T_a (°C)	50
T_c (°C)	50
$T_{dp,a}$ (°C)	40
$T_{dp,c}$ (°C)	40
P_a (psi)	20
P_c (psi)	20
$\dot{V}_a(sccm)$	50
$\dot{V}_c(sccm)$	150

3. Results and discussion

A non-humidified membrane was operated at a current density of 100 mA cm^{-2}, with anode and cathode stoichiometries of 1.5 and 1.8, respectively. The low current density used reduced the stress on membrane during conditioning, while the water generated enhanced the humidification process. The cell voltage during membrane conditioning is shown in Fig. 3. It can be seen that the small load placed on a not conditioned membrane results in an initial zero voltage. As water is produced on the cathode side, it humidifies the membrane and the cell voltage increases to a steady state voltage of about 0.8 V.

To study the dynamics of liquid water during membrane conditioning, the sensory vessel of Fig. 1 was placed at the output of the fuel cell cathode. In order to increase the water carrying capacity of the stream that passes through the vessel and allow evaporating the liquid water that exits the fuel cell and accumulates in the vessel into the stream, the vessel was heated to 90 °C, i.e., 10 °C above the fuel cell temperature. The tubing that connected the vessel and the cathode output were also heated to the same temperature to prevent condensation. In Fig. 4a, the vessel temperature and dew point measurement readings, T_v and T_{dp}, from 500 s after imposing load on the fuel cell is shown.

It is seen in Fig. 4a that there are two steady state levels for the dew point temperature, one around 70 °C and the other around 85 °C. With the cathode output stream temperature measured at 72 °C, the lower dew point temperature corresponds to near saturation pressure of the cathode measured in a dry vessel. The vessel temperature reading in Fig. 4a shows a temperature of about 87 °C, therefore, the higher dew point temperature around 85 °C corresponds to near saturation of the vessel when liquid water is present

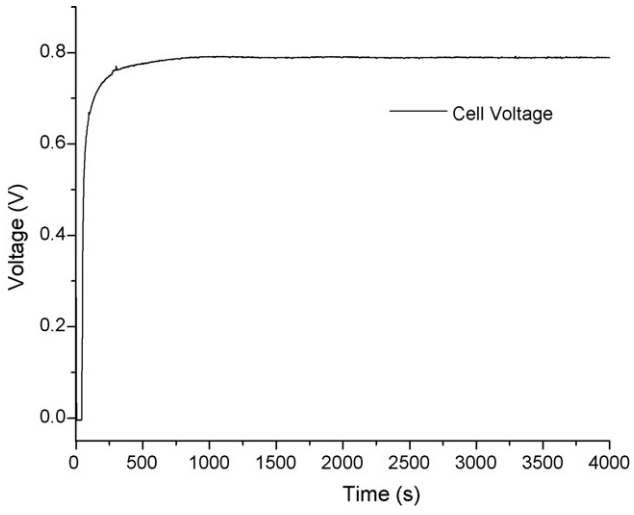

Fig. 3. Fuel cell voltage during membrane humidification at a current density of 100 mA cm^{-2}.

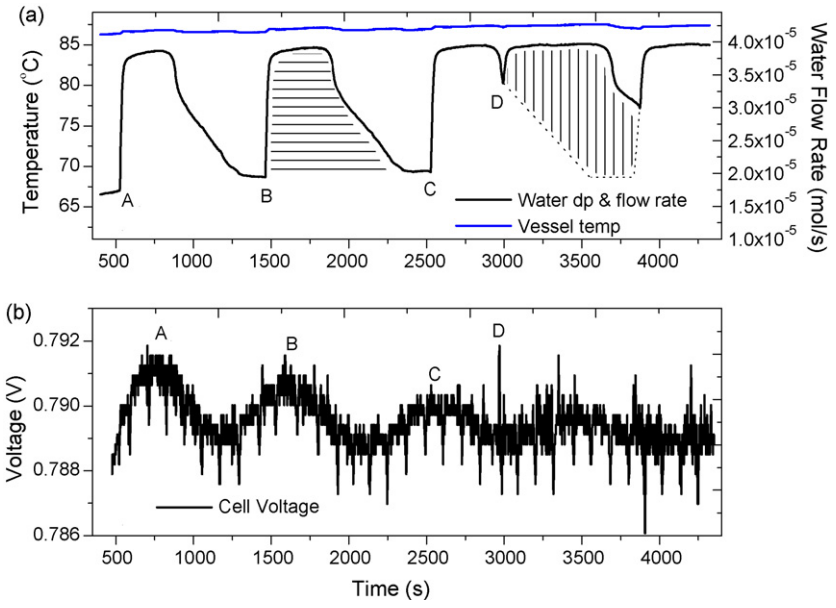

Fig. 4. Dew point temperature and stream temperature of the cathode stream in the humidity sensing vessel (top), and cell voltage (bottom) versus time. The points A, B, C, and D on the top and bottom graphs correspond to the same moment in time. The difference in time observed is due to the accuracy of the different data acquisition systems used to measure the data on the top and bottom graphs. The horizontally and vertically hashed lines correspond to two convective water transport mechanisms by the cathode stream. The output water flow rate on the top graph is calculated from the vessel dew point temperature reading.

in the vessel. Therefore, times A, B, C, and D in Fig. 4a correspond to the time at which liquid water is expelled from the cathode into the vessel, causing a jump in the vessel dew point temperature.

At the right axis of Fig. 4a, the molar flow rate of water vapor exiting the vessel, $\dot{n}_{vap}$, calculated from the air flow rate, pressure, and vessel dew point temperature using Eq. (4) is also marked. On this axis, the area below the 70 °C dew point temperature (2×10^{-5} mol^{-1}) corresponds to the amount of water that exits the cathode in vapor form, while the area between this dew point temperature and 85 °C (4×10^{-5} mol^{-1}) corresponds to amount of water that exit the fuel cell in liquid form. Note that in Fig. 4a, when all the liquid water in the vessel is evaporated and the vessel dries, the dew point temperature has an initial sharp drop, followed by a slow decay in the dew point temperature, until it reach the saturation dew point temperature of the cathode. This is due to the dilution effect of the input stream into the vessel.

The net rate of water production in the fuel cell cathode at 100 mA cm^{-2} is 2.54×10^{-5} mol^{-1}. The net rate of water evaporation in the cathode can be calculated as the difference between the cathode input and output water vapor molar flow rates, using the cathode input and output partial pressures and flow rates in Eq. (4), to be 1.62×10^{-5} mol^{-1}. This results in an average liquid water accumulation in the cathode of about 0.92×10^{-5} mol^{-1}. The periodic liquid water that is released from the cathode has an average value about 0.95×10^{-5} mol^{-1}, well in agreement with the calculated amount.

The fuel cell voltage is graphed in Fig. 4b for $t > 500$ s, which reveals a decaying voltage oscillation. These oscillations cannot be seen over the same period in Fig. 3 due to their small amplitude (less that 0.5% of the steady state). The peak of cell voltage oscillations in Fig. 4b is marked with times A, B, and C, which correspond to times A, B, C, in Fig. 4a where liquid water is expelled out of the fuel cell cathode. The slow dynamics of these voltage oscillations (period around 1070 s) suggest that it corresponds with changes in membrane/ionomer humidification conditions in the cathode. The decreasing amplitude of the low frequency voltage oscillations could also result from a better humidified membrane, being less affected by the liquid water leaving the cathode. Also the presence of liquid water in the cathode means that we have a fully saturated cathode stream, therefore, the fact that liquid water leaving the cathode at times A, B, and C deteriorates membrane humidification conditions suggest that the liquid water is in direct contact with the membrane in the cathode, i.e., catalyst/GDL boundary. It is also seen in Fig. 4a that the amount of liquid water expelled from the cathode at times A, B, and C are almost equal. This suggests that when the liquid water reaches a critical mass, the convective forces dominate the forces attaching the water droplets to the GDL, resulting in their detachment. This hypothesis is in line with the observation of authors in [31,32].

The amount of liquid water expelled from the cathode into the vessel between two dry vessel states, e.g., B and C in Fig. 4a, can be calculated from Eq. (1), with points B and C representing times t_1 and t_2, respectively. This amount is shown in Fig. 4a as the area of the horizontally hashed region calculated using the left vertical axis (molar flow rate of water vapor through the vessel) and the horizontal axis (time), which results in a total amount of liquid water about 10^{-2} mol, or equivalently 0.18 cm^3. Assuming that all this water is in the GDL, with a cell area of 49 cm^2 and GDL porosity of 50%, this volume would fill an average depth of 73 μm. This is comparable with the GDL thickness around 170 μm. Therefore, it is feasible for the periodic liquid water that affects the membrane/ionomer humidification conditions to originate from the GDL.

In Fig. 4a, water is also expelled out of the fuel cell at time D. However, in Fig. 4b, this corresponds with a spike in the cell voltage, which suggests that the source and dynamics of liquid water leaving the fuel cell at time D is different than that of at times A, B, and C. The transient spike suggests that the liquid water released at point D originates from the flow field and manifolds. This water blocks the flow fields and its release creates a sudden pressure drop that temporarily opens that GDL and catalyst pores from liquid water, allowing more oxygen to reach the reaction sites and therefore a spike in cell voltage. This is in line with the observation of authors in [22] that showed a sudden voltage jump could result from depletion of water from the cathode flow field. Note that the total amount of liquid water that is released at point D is shown in Fig. 4a by the vertically hashed area, and is about 10^{-2} mol, or equivalently 0.18 cm^3, which is well within the range of the cathode and manifold volume of about 6 cm^3.

4. Conclusions

In this paper, a sensory system was presented capable of measuring two-phase flow of water as it exits the fuel cell. The sensory system was placed at the output of a PEFC cathode to study the transport of water during the membrane conditioning process. Two distinguish modes of liquid water transport out of the cathode was observed: the first mode was periodic, with a period equal to that of the fuel cell voltage oscillations. The slow time constant and the decaying periodic voltage oscillation suggest that it corresponds to the membrane/ionomer humidification conditions. The second mode of liquid water transport corresponds with a spike in the cell voltage, which suggests that the liquid water originated from the flow field and manifold. Therefore, we conclude that this sensory system can be used to better understand and quantify two-phase flow in the fuel cell, which is essential for design optimization.

References

[1] J. Larminie, A. Dicks, Fuel Cell Systems Explained, John Wiley & Sons, 2000.
[2] T.E. Springer, T.A. Zawodzinski, S. Gottsfeld, J. Electrochem. Soc. 138 (1991) 2334–2341.
[3] J.M. Le Canut, R.M. Abouatallah, D.A. Harrington, J. Electrochem. Soc. 153 (5) (2006) A857–A864.
[4] F. Weng, A. Su, C. Hsu, Int. J. Hydrogen Energy 32 (6) (2007) 666–676.
[5] A. Kulikovsky, H. Scharmanna, K. Wippcrrnann, Electrochem. Commun. 6 (2004) 729–736.
[6] Y. Wang, S. Basu, C. Wang, J. Power Sources 179 (2) (2008) 603–617.
[7] H. Liu, L. You, J. Power Sources 155 (2) (2006) 219–230.
[8] M. Acosta, C. Merten, G. Eigenberger, H. Class, R. Helmig, B. Thoben, H. Muller-Steinhagen, J. Power Sources 159 (2) (2006) 1123–1141.
[9] L. You, H. Liu, Int. J. Heat Mass Transfer 45 (11) (2002) 2277–2287.
[10] T. Berning, N. Djilali, J. Electrochem. Soc. 150 (12) (2003) A1589–A1598.
[11] M. Eikerling, J. Electrochem. Soc. 153 (3) (2006) E58–E70.
[12] Y.W. Rho, S. Srinivasan, Y.T. Kho, J. Electrochem. Soc. 141 (8) (1994) 2089–2096.
[13] G. Lin, W. He, T.V. Nguyen, J. Electrochem. Soc. 151 (12) (2004) A1999–A2006.
[14] Z. Dunbar, R.I. Masel, J. Power Sources 171 (2) (2007) 678–687.
[15] Z. Zhang, J. Martin, J. Wu, H. Wang, K. Promislow, B.J. Balcom, J. Magn. Resonan. 193 (2) (2008) 259–266.
[16] J. Bedet, G. Maranzana, S. Leclerc, O. Lottin, C. Moyne, D. Stemmelen, P. Mutzenhardt, D. Canet, Int. J. Hydrogen Energy 33 (12) (2008) 3146–3149.
[17] K. Teranishi, S. Tsushima, S. Hirai, J. Electrochem. Soc. 153 (4) (2006) A664–A668.
[18] F.Y. Zhang, X.G. Yang, C.Y. Wang, J. Electrochem. Soc. 153 (2) (2006) A225–A232.
[19] A. Hakenjos, H. Muenter, U. Wittstadt, C. Hebling, J. Power Sources 131 (1) (2004) 213–216.
[20] K. Tüber, D. Pócza, C. Hebling, J. Power Sources 124 (2) (2003) 403–414.
[21] D. Spernjak, A.K. Parsard, S.G. Advani, J. Power Sources 170 (2) (2007) 334–344.
[22] X. Liu, H. Guo, C. Ma, J. Power Sources 156 (2) (2006) 267–280.
[23] T. Ous, C. Arcoumanis, J. Power Sources 173 (1) (2007) 137–148.
[24] A. Turhan, K. Heller, J.S. Brenizer, M.M. Mench, J. Power Sources 160 (2) (2006) 1195–1203.
[25] D.S. Hussey, D.L. Jacobson, M. Arif, J.P. Owejan, J.J. Gagilardo, T.A. Tarbold, J. Power Sources 172 (1) (2007) 225–228.
[26] J.J. Kowal, A. Turhan, K. Heller, J. Brenizer, M.M. Mench, J. Electrochem. Soc. 153 (10) (2006) A1971–A1978.
[27] J. Zhang, D. Kramer, R. Shimoi, Y. Ono, E. Lehmann, A. Wokaun, K. Shinohara, G.G. Scherer, Electrochim. Acta 51 (2006) 2715–2727.
[28] I.A. Schneider, D. Kramer, A. Wokaun, G.G. Scherer, Electrochem. Commun. 7 (12) (2005) 1393–1397.
[29] T.A. Trabold, J.P. Owejan, D.L. Jacobson, M. Arif, P.R. Huffman, Int. J. Heat Mass Transfer 49 (25) (2006) 4712–4720.
[30] N. Pekula, K. Heller, P.A. Chuang, A. Turhan, M.M. Mench, J.S. Brenizer, K. Ünluü, Nucl. Instrum. Meth. Phys. Res. Sect. A 542 (1–3) (2005) 134–141.
[31] M.W. Renfro, S. Basu, H. Gorgun, B.M. Cetegen, J. Power Sources 159 (2) (2006) 987–994.
[32] S. Basu, M.W. Renfrow, B.M. Cetegen, J. Power Sources 162 (1) (2006) 286–293.
[33] T. Fabian, R. O'Hayre, F.B. Prinz, J.G. Santiago, J. Electrochem. Soc. 154 (9) (2007) B910–B918.
[34] G.Q. Lu, F.Q. Liu, C. Wang, J. Power Sources 164 (1) (2007) 134–140.
[35] M.M. Mench, Q.L. Dong, C.Y. Wang, J. Power Sources 124 (1) (2003) 90–98.
[36] X. Yang, N. Burke, C. Wang, K. Tajiri, K. Shinohara, J. Electrochem. Soc. 152 (4) (2005) A759–A766.
[37] Q. Yan, H. Toghiani, J. Wu, J. Power Sources 158 (1) (2006) 316–325.
[38] A. Schmitz, M. Tranitz, S. Eccarius, A. Weil, C. Hebling, J. Power Sources 154 (2) (2006) 437–447.
[39] H. Nishikawa, R. Kurihara, S. Sukemori, T. Sugawara, H. Kobayasi, S. Abe, T. Aoki, Y. Ogami, A. Matsunaga, J. Power Sources 155 (2) (2006) 213–218.
[40] P. Berg, K. Promislow, J. St. Pierre, J. Stumper, B. Wetton, J. Electrochem. Soc. 151 (3) (2004) A341–A353.